Ultra-Wideband Statistical Channel Model for Non Line of Sight Millimeter-Wave Urban Channels

Mathew K. Samimi, Theodore S. Rappaport
NYU WIRELESS, New York University
Brooklyn, NY
mks@nyu.edu, tsr@nyu.edu

***Abstract*—This paper presents ultra-wideband statistical spatial and omnidirectional channel models for 28 GHz millimeter-wave cellular dense urban Non-Line of Sight (NLOS) environments, developed from wideband measurements in New York City that used synthesized timing from 3D ray-tracing. An accurate 3GPP-like channel model has been developed, where model parameters are based on empirical distributions for time cluster and spatial (lobe) channel parameters. A statistical simulator capable of reproducing the joint temporal and spatial measured channel statistics is given here. A step-by-step procedure for generating channel coefficients is shown to validate measured statistics from 28 GHz field measurements, thus validating our statistical channel model, for use in standard bodies and system-level simulations for millimeter-wave wideband communications.**

Keywords—Millimeter-Wave; Dense environment; NLOS; statistical spatial channel models; Wideband; 3D Ray-tracing; statistical simulator; cluster; lobe.

I. INTRODUCTION

The demand for greater data rates is expected to increase 1000-fold by the year 2020. The millimeter-wave (mmWave) spectrum offers an enormous amount of bandwidth that will deliver multi-Gigabit-per-second data rates to mobile phones [1]. The use of highly directional antennas at the transmitter and receiver will compensate for greater free space path loss at mmWave frequencies, while atmospheric and rain attenuations are minimal over a cell radius of 200 m for 28 GHz [2] [3].

Radio-system designers require a statistical spatial channel model (SSCM) to study different physical layer (PHY) phenomena and to develop hardware and algorithms for future mmWave devices and systems [4]. Statistical models also avoid the need for additional costly and time-consuming propagation measurements, and help the standardization process for radio-system design throughout the world.

Current 3G and 4G MIMO radio-systems are designed using the geometry-based stochastic 3GPP and WINNER II statistical spatial channel models (SSCM). These models are based on empirical studies between 1 and 6 GHz, and for RF bandwidths between 5 and 100 MHz, and provide important statistical channel parameters such as multipath delays, cluster powers, angle of arrival (AOA) and angle of departure (AOD) information, as well as path loss models based on real-world measurements, and also produce complex channel coefficients for simulating channel impulse responses [5] [6]. While these two channel models have been successful in describing the stochastic nature of the low frequency (UHF/microwave) channels, they are not based on ultra-wideband mmWave measurements, and do not distinguish spatial AOAs (lobes) that can have energy arriving from multiple propagation time clusters within the same spatial lobe.

The lack of 28 GHz SSCM for outdoor dense urban environments motivated our measurements in New York City to characterize wideband mmWave channels for future wireless communications. We conducted extensive propagation measurements in dense urban LOS and NLOS environments in Manhattan and measured 75 TX-RX location combinations for three distinct TX locations with distances up to 500 m [2] [3]. We found that LOS channels are very much like free space when directional antennas are used, thus we focus here on the NLOS measurements and models, as these pose the greatest challenge for mmWave systems. Our measurements used a 400 mega-chips-per-second (Mcps) broadband sliding correlator channel sounder and 24.5 dBi (10.9° and 8.6° 3-dB beamwidths in azimuth and elevation, respectively) rotatable horn antennas, and transmitted an 800 MHz RF first null-to-null bandwidth signal centered around 28 GHz to study the dispersive nature of dense urban wireless channels [2]. Over 4,000 power delay profiles (PDPs) were collected for wideband temporal and AOA and AOD statistics, which are used here to develop omnidirectional channel models, similar to the 3GPP and WINNER II models. Such statistical models are required for characterization of the 28 GHz ultra-wideband dense urban propagation channel, and the first such known model is presented here, based on the measurements in [2].

II. SYSTEM LIMITATIONS AND 3D RAY-TRACING

The 28 GHz measurements and the sliding correlator measurement system with rotating horn antennas are described in [2][3]. The absence of GPS synchronization between TX and RX prevented us from recovering absolute propagation time with each PDP, as only excess delay (relative to the first arriving multipath) was measured. We needed a way to synthesize absolute arrival times for every PDP to create an omnidirectional SSCM. As illustrated in Fig. 1, a true omnidirectional channel impulse response requires knowledge of absolute time of all arriving multipath components over all angles. The limitation of our measurement system was remedied in post-processing using three-dimensional (3D) ray-tracing techniques to synthesize absolute propagation times at all NLOS RX locations, where the shortest propagation time between TX and RX was recovered at different receiver

978-1-4799-3512-3/14/$31.00 ©2014 IEEE

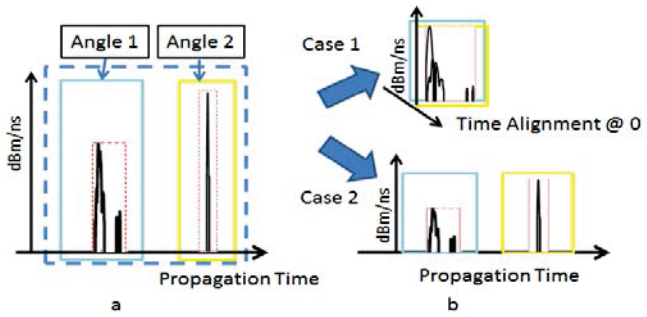

Fig. 1: a) True Power Delay Profile (PDP) resulting from multipath arriving from two different Angles of Arrivals (AOAs) at a particular RX location. The multipath signals arriving from Angle 1 arrive before those of Angle 2. Case 1 b) shows how the measured PDPs from our measurement system [2][3] uses excess delay, and not absolute propagation delay, and thus was unable to discern the true propagation delays of multipath arriving from different angles. To solve this problem, ray-tracing was performed at each RX location to allow time alignment with absolute timing of multipath signals for every prominent AOA. Case 2 shows how, through the use of ray-tracing, the superposition of PDPs at different angles can distinguish absolute propagation times across different pointing angles, as is needed for accurate SSCMs [7].

azimuth angles, and used to appropriately superimpose the true propagation time on all measured PDPs. Google SketchUp was used to model a 3D geographical database of the measured Manhattan environment (over a 800 x 800 m^2 area) and we developed a 3D ray-tracing software in MATLAB to emulate electromagnetic propagation for arbitrary antenna patterns. The ray-tracer implemented the law of reflection and a simple radar cross section (RCS) scattering model to account for diffuse scattering. Rays that matched the measurement locations and antenna orientations (in 3D) were computed to determine propagation time delays for up to four most prominent AOAs for each NLOS RX location, and these absolute propagation times were all that we needed for proper superposition (see Fig. 1). We chose the four strongest AOAs (although some locations had fewer strong AOAs) to determine absolute timing through ray-tracing, realizing that most of the power in any PDP is received in the strongest few azimuth directions, and further work would offer diminished value [8].

I. Extracting Channel Models from Measurements

A. Omnidirectional NLOS Path Loss Model

While quite extensive, our 28 GHz field measurements were not truly omnidirectional, in that highly directional horn antennas were used to obtain sufficient link margin, and only one elevation angle and three azimuthal pointing angles were used at the transmitter while the RX was swept in azimuth. Furthermore, when the RX azimuth sweeps were made, there were only three different elevation angles used at the RX. For the case where the TX was rotated over all azimuth directions at a single down tilt angle, a single RX pointing angle was used. However, this procedure [2][3] was crafted to assure that most of the energy (e.g. reasonably close to a true omnidirectional situation) would be measured. For the RX sweeps, it had been shown earlier (and was further verified in the 28 GHz measurements) that most of the energy arriving at the RX comes from a relatively small azimuthal range of TX antenna orientations [9]. Since the 24.5 dBi TX antennas had 10˚ beamwidths, the powers summed at the RX's contained some overlapping energy from each of the three TX orientations, since the TX azimuth angles used in the RX sweep measurements were spaced 5° (a half-beamwidth) apart from each other [2][3]. This is justified by the fact that only one TX elevation angle was used in the field, hence the generous received power due to the closely-spaced (partially overlapped) TX azimuth antenna patterns would be offset by the dearth of power due to the fact that no other TX elevation orientations were measured in the field. From these synthesized omnidirectional PDPs, we extracted omnidirectional path losses by finding the received power (area under the omnidirectional PDPs) at each RX location, and removing antenna gains from the received power (we were careful not to double count power from the many TX and RX sweeps at each location). We then found the corresponding large scale omnidirectional path loss model from the resulting received power levels at each RX location.

Fig. 2 shows the omnidirectional 28 GHz large scale path loss with respect to a 1 m free space, where the omnidirectional path loss is obtained from all of the measured powers from all PDPs measured over all angles at both the TX and RX, with antenna gains deducted from each measured PDP. The measured data yields an omnidirectional measured path loss exponent and shadowing factor (with respect to a 1 m free space reference) of $n_{All} = 3.4$ and $\sigma_{All} = 9.7\,dB$, respectively, yielding a large scale path loss model of

$$PL[dB](d) = 61.4 + 34\log_{10} d + \chi_{\sigma} \quad (1)$$

Note that when using just the few strongest measured PDPs at each RX location, with synthesized absolute propagation time included providing an omnidirectional PDP, the synthesized timing approach yields a path loss exponent of $n_{Syn} = 3.7$ and shadowing factor $\sigma_{Syn} = 12.3\,dB$, thus agreeing reasonably well (variation of only 3 dB per decade of distance) with the omnidirectional path loss model developed from all of the measured PDPs over all angles (note: our SSCM uses the field measured path loss exponent and shadowing values). This clearly illustrates how just a few key AODs and AOAs provide most of the energy in an urban mmWave channel. For completeness, a floating intercept path loss model from 30 to 200 m determined from all of the measured data, and used in a mmWave capacity analysis [10] is also shown on Fig. 2, illustrating the similarity of these various models.

B. Cluster and Lobe Statistics

The two principal SSCM modeling concepts used here are *time cluster* and *spatial lobe;* these deal with the temporal (i.e., omnidirectional) and spatial components of the statistical channel model, respectively [7]. Fig. 3 and Fig. 4 illustrate cluster and lobe terminology. A time cluster is defined as a group of cluster subpaths (i.e., multipath components) traveling closely in time and space. Temporal cluster statistics are described by nine cluster parameters, including the absolute time of arrival, the azimuth and elevation angles of

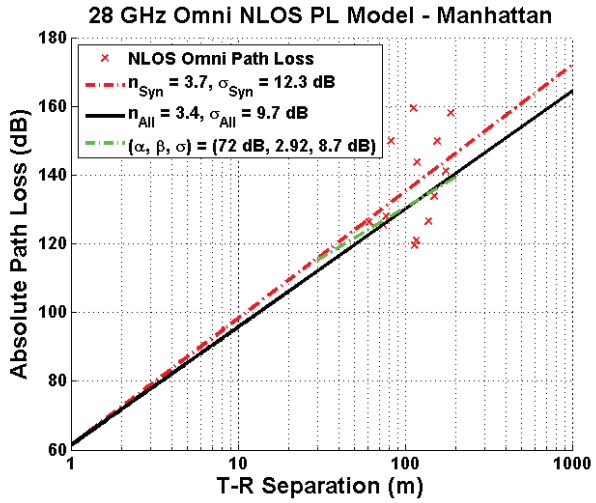

Fig. 2: Omnidirectional path loss models are shown here, obtained from the wideband measurements in Manhattan. The omnidirectional power at each NLOS RX location was obtained from all PDPs for all RX and TX pointing angles (but double counts were eliminated), and antenna gains were removed from each PDP. The path loss exponent and shadowing factor obtained when summing all received powers at all azimuth and elevation angles are 3.4 and 9.7 dB, respectively, using a 1 m free space reference distance. The floating intercept type model for 28 GHz, (similar to the form used in 3GPP) is shown in green between 30-200 m [10]. The synthesized omnidirectional PDPs using only up to four measured PDPs (the most prominent AOAs) yield a path loss exponent and shadowing factor (with respect to a 1 m free space reference) of 3.7 and 12.3 dB (red line), showing good agreement to field measurements.

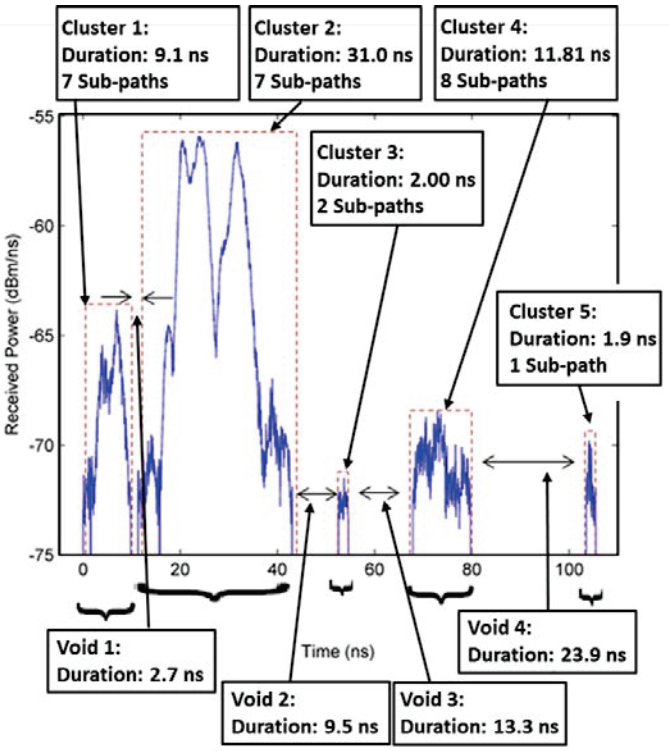

Fig. 3: Shown is a typical power delay profile measured in Manhattan at 28 GHz with energy arriving from a particular AOA. Measurements were made with rotating directional horn antennas in 10˚ azimuth steps and a few different elevation angles at the RX [2][3]. Here, the temporal cluster terminology is illustrated. Five time clusters may be seen with time durations ranging from 2 ns to 31 ns.

departure, the azimuth and elevation azimuth and elevation angles of arrival, and the azimuth and elevation spreads of arrival. A spatial lobe is defined as a departing or incoming direction of contiguous energy over the azimuth and/or elevation planes, and is identified by eight principal lobe parameters: the azimuth and elevation angles of departure, the azimuth and elevation spreads at the transmitter, the azimuth and elevation angles of arrival, and the azimuth and elevation spreads at the receiver [7][8]. The mmWave measurements in [2] show that several temporal clusters may arrive in the same spatial lobe at the RX, thus we believe it may be useful to add an additional feature of correlating time with angular space when describing mmWave channels, as opposed to current 3GPP and WINNER II models that assign one time cluster to only one AOA. Those wishing to ignore our lobe definition will find that our models are identical to 3GPP and WINNER models, and lobe statistics (power over space) are harmonized to give accurate temporal results whether or not the lobe statistics are used in the model, since the total power in the lobes is made identical to the total power captured in the time clusters (e.g. the power over space is identical to the power over time).

In order to develop a statistical simulator capable of recreating omnidirectional impulse responses or PDPs with proper azimuth spectra, key statistics were identified from measured data as shown in Table II and Table III. Many statistics are possible, but, some have only indirect impact on the generated PDPs. For example, modeling the statistical spreads of departure, the distribution describing RMS delay

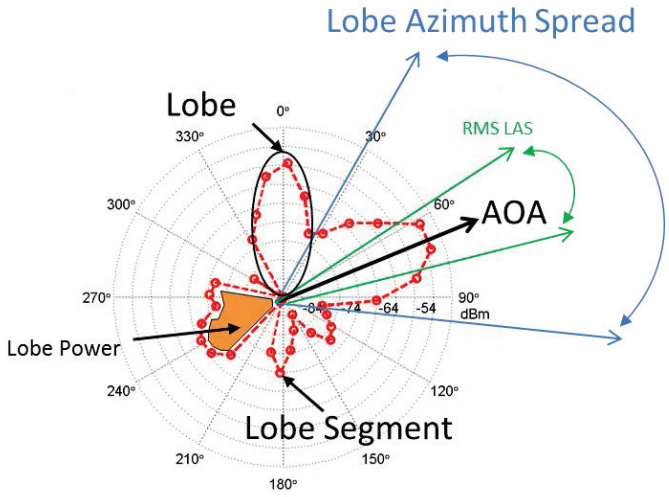

Fig. 4: Shown is a polar plot measured in Manhattan at 28 GHz, where our lobe terminology is illustrated. Five distinct lobes may be seen with various lobe azimuth spreads and AOAs. Each red 'dot' is a lobe angular segment measured at a particular pointing angle, and represents the total integrated received power over a 10˚ angle (e.g. the area under a PDP for a particular RX pointing angle). The lobe power is the sum of powers from each segment within the lobe (e.g. the sum of powers from each lobe segment in a lobe).

spread of omnidirectional PDPs is a useful exercise for verifying gross accuracy of the simulation methodology but does not help in actually generating a PDP, since the RMS delay spread itself depends on more fundamental channel

quantities needed to design modems and determine algorithms, namely, the power levels and time of arrivals of individual multipath components in the PDP. We therefore refer to *primary statistics* for generating channel impulse response coefficients, and *secondary statistics*, such as RMS delay spread, when describing statistics used to test the validity and accuracy of the statistical simulator. All primary cluster and lobe statistics are identified in Tables II and III. The number of time clusters and cluster subpaths in an omnidirectional profile were found by counting the number of groups of closely spaced multipath components, and the number of subpath components in each cluster, after applying an appropriate cluster partitioning algorithm. The cluster excess time delay corresponds to the time of arrival of the first subpath component composing a time cluster, relative to the time of arrival of the first arriving cluster. The cluster subpath excess time delay, or intra-cluster time delay, corresponds to the time of arrival of a subpath component within a time cluster, relative to the first arriving sub-path component in the same cluster. The relative cluster (cluster subpath) power levels correspond to the fraction of power contained in a cluster (cluster subpath) with respect to the total power contained in the omnidirectional PDP (time cluster). The cluster powers were studied by considering the ratio between the total cluster power (in linear units) and the total power in the omnidirectional profile (in linear units). Each cluster and cluster subpath power ratio thus lies between a value of 0 and 1 [7] [8]. The number of lobes in a polar plot corresponds to the number of outgoing or incoming energy directions at the transmitter or receiver, respectively. The azimuth spread of a lobe is defined as the azimuth angle span over which the lobe exists. The AOA of a lobe is defined as the power weighted mean angle of the lobe power azimuth spectrum (PAS). The lobe segment power ratios correspond to the fractional amount of power in each lobe segment with respect to the maximum power segment in the lobe [7][8].

C. Cluster Partitioning and Lobe Thresholding

The statistics corresponding to time clusters and spatial lobes are dependent upon the cluster partitioning scheme used on PDPs and upon the thresholding procedure used on PAS, respectively. Spatial lobes, also referred to as spatial clusters in [10], are an improvement over 3GPP models as the proposed mmWave channel model explicitly differentiates spatial arrivals of energy within an observable temporal cluster, providing additional dimensionality for researchers. The mean number of lobes was found to be 1.8 using a *k*-means clustering algorithm in [10], where [10] lumped all of our 28 GHz LOS and NLOS measurements into one dataset (LOS locations have fewer spatial lobes than NLOS, as described in [7]). For NLOS locations, we obtained an average of 2.4 distinct angular lobes when applying a 20 dB threshold below maximum received power levels on the PAS, as in [7].

To create the SSCM, the number of clusters and number of cluster subpaths were fit to a Poisson and Exponential distributions (see Steps 3 and 4 of II.A), respectively, by realizing that the number of clusters in an omnidirectional PDP is negatively correlated with the number of cluster subpaths. Indeed, as the minimum inter-cluster void duration (minimum void interval between two consecutive time clusters) increases, the number of clusters in an omnidirectional PDP must decrease, and therefore the number of subpaths per cluster must increase, and vice-versa. The general skewness of these two distributions will tend to be opposite. A natural first attempt at modeling the number of clusters and the number of subpaths per cluster was therefore to choose a Poisson distribution and a Discrete Exponential distribution, which exhibit opposite skewness.

The optimum inter-cluster void duration (void durations are shown in Fig. 3) was obtained by simultaneously minimizing the χ^2 criterion between the expected (pre-determined) distributions and the computed statistics, as given by [11]:

$$\chi^2 = \sum_{i=1}^{k} \frac{(n_i - E_i)^2}{E_i} \qquad (2)$$

where n_i is the number of observations and E_i is the expected number of observations for the i^{th}class.

The optimization was performed numerically by computing the probability mass densities for the number of clusters and the number of cluster subpaths by varying the inter-cluster void interval over the ensemble of omnidirectional PDPs (see Fig. 3). In this work, the optimum inter-cluster void interval was determined to be 2.7 ns, and was used to produce the entire set of temporal and spatial statistics. Fig. 5 and Fig. 6 show the measured distributions for the number of clusters and the number of cluster subpaths in omnidirectional profiles, after applying a 2.7 ns inter-cluster time duration on the entire ensemble of omnidirectional PDPs. The mean number of time clusters and cluster subpaths were found to be 3.4 and 1.2 respectively. Fig. 7 shows the measured distribution for the number of AOA lobes found at all NLOS RX locations, after applying a 20 dB threshold on measured PAS.

D. Wideband Channel Models

Table II and Table III, Columns 2 and 3, summarize the primary and secondary statistics extracted from the time synthesized omnidirectional PDPs and measured PAS. In all cases, a χ^2 goodness of fit test with significance level of 5% was performed to ensure a close fit between the measured and corresponding theoretical distributions (see Section II.A).

II. Statistical Simulator and Generating Channel Coefficients

A. Step Procedure for Generating Channel Coefficients

An accurate omnidirectional channel statistical simulator should be able to generate a collection of PDPs and PAS which, when viewed as a statistical ensemble, recreate the statistics of the measured channels [12]. The extracted channel parameters given here generate key primary statistics that properly generate omnidirectional PDPs and PAS that are identical (in a statistical sense) to actual field measurements in 28 GHz wideband dense urban NLOS channels. To validate the channel models, a MATLAB-based statistical simulator was created, based upon the following step-by-step procedure for generating channel coefficients. The models are valid for

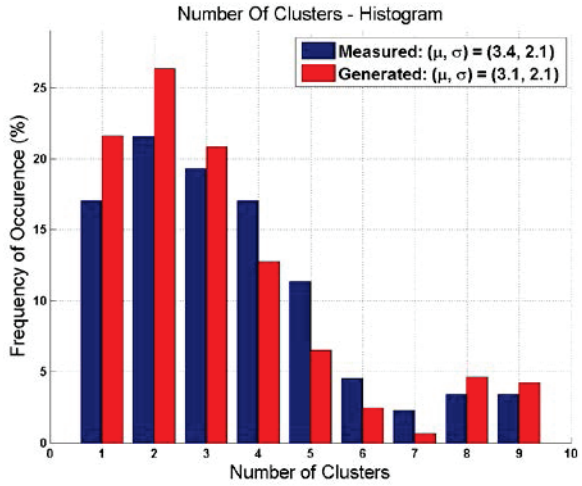

Fig. 5: Histogram of the number of time clusters in NLOS omnidirectional power delay profiles obtained using a 2.7 ns minimum inter-cluster void interval. The blue bars correspond to the measured frequency of occurrence. The red bars were generated based on the simulation procedure outlined in A, Step 3, showing good agreement to measurements.

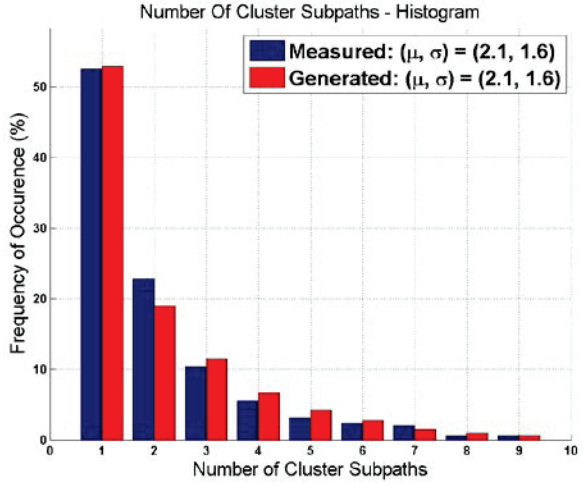

Fig. 6: Histogram of the number of subpaths in a time cluster in NLOS omnidirectional power delay profiles obtained using a 2.7 ns minimum inter-cluster void interval. The blue bars correspond to the measured frequency of occurrence. The red bars were generated based on the simulation procedure outlined in A, Step 4, showing good agreement to measurements.

the types of channels measured in [2], [3], and assume a carrier frequency of 28 GHz, an RF channel bandwidth up to 800 MHz in a dense urban NLOS environment, with obstructions between the TX and RX. The step procedure for generating temporal and spatial profiles is provided below. We note that Step 11 bridges the temporal and spatial components of the SSCM by associating temporal cluster powers to the directions of strongest arriving power; a similar feature was used in previous 3GPP or WINNER models, but we keep the PAS.

Step 1. Generate the T-R Separation distance d ranging from 60-200 m (based on our NLOS field measurements, and could be modified with further measurements):

$$d \sim U(d_{min} = 60\ m, d_{max} = 200\ m)$$

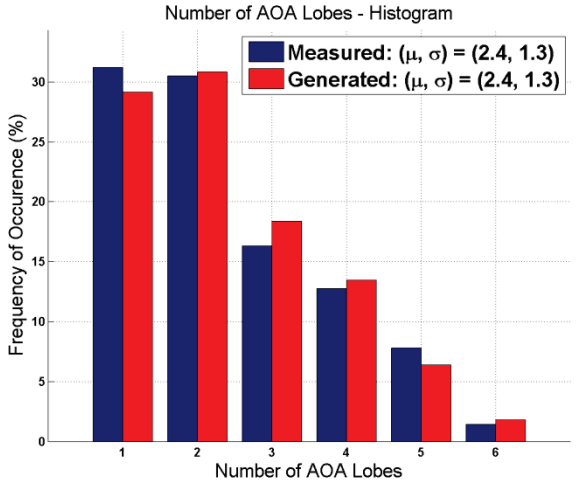

Fig. 7: The histogram of the number of AOA lobes measured at all NLOS RX location from the 28 GHz wideband collected measurements in Manhattan. The mean and standard deviation of the number of AOA lobes were 2.4 and 1.3 respectively. The red bars were generated based on the procedure outlined in Section A.

Note: To validate our simulation, we used a U(60,200), but for standards work any distance less than 200 m is valid.

Step 2. *Generate the total received power Pr (dBm) at the NLOS RX location:*

$$Pr[dBm] = P_t + G_t + G_r - PL[dB]$$

$$PL[dB] = PL(d_0) + 10\bar{n}log_{10}\left(\frac{4\pi d}{\lambda}\right) + \chi_\sigma$$

$$PL(d_0) = 20\,log_{10}\left(\frac{4\pi d_0}{\lambda}\right) = 61.4\ dB$$

$$\chi_\sigma \sim N(\mu = 0\ dB, \sigma = 9.6\ dB)$$

P_t is the transmit power in dBm, G_t and G_r are the TX and RX antenna gains respectively, $d_0 = 1$ m, $\lambda = 0.0107$ m, and $\bar{n} = 3.41$ for omnidirectional TX and RX antennas in NLOS channels. χ_σ is lognormal with 0 dB mean, $\sigma = 9.6$ dB.

Step 3. Generate the number of time clusters N and the number of spatial lobes L at the RX location:

$$N = \max(1, A_1)$$

$$L = \begin{cases} \max(1, B_1), & B_1 \le N \\ N, & B_1 > N \end{cases}$$

where: (X, Y, Z) ~ U(0,1)

$$A_1 = \begin{cases} A_2, & A_{Temp} = 1 \\ A_3, & A_{Temp} = 3 \\ 7, & A_{Temp} \ge 10 \\ A_{Temp}, & \text{Otherwise} \end{cases}$$

$$A_2 = \begin{cases} 1, X > 0.8 \\ 8, X \le 0.2 \end{cases} \quad A_3 = \begin{cases} 3, Y > 0.85 \\ 9, Y \le 0.15 \end{cases}$$

$$A_{Temp} \sim Poisson(\mu = \mu_N - 0.5)$$

$$B_1 = \begin{cases} B_2, & B_{Temp} = 3 \\ 5, & B_{Temp} \ge 7 \\ 1, & B_{Temp} = 5 \\ B_{Temp}, & \text{Otherwise} \end{cases} \quad B_2 = \begin{cases} 1, Z \ge 0.8 \\ 3, Z < 0.2 \end{cases}$$

$$B_{Temp} \sim Poisson(\mu = \mu_L + 1.5)$$

where $\mu_N = 3.4$ and $\mu_L = 2.4$, the average number of time clusters in an omni PDP, and average number of lobes observed at a RX location, respectively. Note the number of

lobes is always less than or equal to the number of time clusters, and this step assures there is always at least one time cluster and one lobe for every instance.

Step 4. Generate the number of cluster sub-paths M_n in each time cluster:

$$M_n = \begin{cases} \max(1, A), & 1 \le A \le 9 \\ 1, & A \ge 10 \end{cases}$$

where: $A \sim [Exp(\mu = 2.1)]$

Step 5. Generate the intra-cluster subpath excess delays $\rho_{m,n}$ (ns):

$$\rho_{m,n} = 2.5 \times (m-1), m = 1,2,\dots M_n, n = 1,2,\dots N$$

Step 6. Generate the cluster delays τ_n (ns) in conjunction with the cluster sub-path delays generated in Step 4:

$$\tau_n' \sim Exp(\mu = r_\tau \mu_\tau)$$
$$\tau_n'' = \tau_n' - min(\tau_n'), n = 1,2,\dots N$$
$$\tau_n = \rho_{M_n,n-1} + \tau_n'' + 2.7$$

where $\mu_\tau = 67\ ns$ is the observed average cluster excess time delay in an omnidirectional PDP, and $r_\tau = 0.25$ is the delay proportionality constant. This step assures no temporal cluster overlap with a 2.7 ns inter-cluster void.

Step 7. Generate the cluster path powers P_n (mW):

$$P_n' = 10^{\frac{Z}{10}} \alpha e^{-\frac{\tau_n}{\beta}}$$

Per-cluster Shadowing: $Z \sim N(\mu, \sigma)$

$$P_n = \frac{P_n'}{\sum_{k=1}^{k=N} P_k'} \times Pr[mW]$$

where $\alpha = 0.613$, $\beta = 31.4\ ns$, $\mu = 0\ dB$, $\sigma = 9.4\ dB$. Note: α is a primary parameter that, even though it cancels out, verifies an accurate fit to measured data.

Step 8. Generate the cluster subpath powers $\Pi_{m,n}$ (mW):

$$\Pi_{m,n}' = 10^{\frac{U}{10}} \alpha e^{-\frac{\rho_{m,n}}{\beta}}$$

Per subpath shadowing: $U \sim N(\mu, \sigma)$

$$\Pi_{m,n} = \frac{\Pi_{m,n}'}{\sum_{k=1}^{k=M_n} \Pi_{k,n}'} \times P_n[mW]$$

where $\alpha = 0.966$, $\beta = 6.63\ ns$, $\mu = -0.8\ dB$, $\sigma = 5.1\ dB$. Note: our measurements have much greater temporal and spatial resolution than previous models. Intra-cluster power levels were observed to fall off exponentially over intra-cluster time delay.

Step 9. Recover absolute time delays $t_{m,n}$ (ns) of cluster sub-paths based on T-R Separation distance:

$$t_{m,n} = t_0 + \tau_n + \rho_{m,n}, m = 1,2,\dots M_n, n = 1,2,\dots N$$
$$t_0 = \frac{d}{c}$$

where $c = 3 \times 10^8 m.s^{-1}$ is the speed of light in free space.

Step 10. Generate the mean angles θ_i (°) of the spatial lobes to avoid overlap of lobe angles (per definition):

$$\theta_i = U(\theta_{min}, \theta_{max}), i = 1,2,\dots L$$
$$\theta_{min} = \frac{360(i-1)}{L} \text{ and } \theta_{max} = \frac{360i}{L}$$

Step 11. Assign cluster powers P_n successively to the different lobe angles θ_i based Step 7. This step distributes temporal powers into the spatial domain to match our measured data:

$$P(\theta_1) = max(P_1, P_2, \dots, P_N)$$
$$P(\theta_2) = max(P_1, P_2, \dots, P_{N-1})$$
$$\vdots$$
$$P(\theta_L) = max(P_1, P_2, \dots, P_{N-L})$$

Add the remaining $J = N - L - 1$ clusters powers to the L lobes in a uniformly random fashion. This fit the data well.

Step 12. Generate the number of lobe angular segments K_i to find the angular spread (for azimuth, but will be extended also for elevation): $K_i' \sim N(\mu_{AS}, \sigma_{AS})$, $K_i = \frac{[max(K_i', 10)]}{10}$

where $\mu_{AS} = 34.8°$, and $\sigma_{AS} = 25.7°$ are the observed mean and standard deviation of the lobe azimuth spread for our 10° antenna beamwidths, respectively.

Step 13. Generate the discretized lobe segment azimuth angles $\theta_{j,i}$ (°) for each lobe:

$$\theta_{j,i} = \theta_i + 10k, j = 1,2,\dots,K_i, i = 1,2,\dots,L$$

where: $\begin{cases} k = -\frac{K_i-1}{2}, \dots, -2, -1, 0, 1, 2, \dots, \frac{K_i-1}{2}, & K_i \text{ odd} \\ k = -\frac{K_i}{2} + Y, \dots, -2, -1, 0, 1, 2, \dots, \frac{K_i}{2} - X, & K_i \text{ even} \end{cases}$

$X \sim Discrete\ Uniform(0,1)$, and $Y = 1 - X$

Step 14. Generate the lobe angular segment powers $P(\theta_{j,i})$(mW):

$$P(\theta_{j,i}) = R(\Delta\theta_{j,i}) P(\theta_i), j = 1,2,\dots,K_i, i = 1,2,\dots,L$$

where: $R(\Delta\theta_{j,i}) = exp\left(-\frac{\Delta\theta_{j,i}^2}{2\sigma^2}\right), \sigma = 11.5°$ $\Delta\theta_{j,i} = |\theta_{j,i} - \theta_i|$

B. Comparison between Measured and Simulated Statistics

An ensemble (10,000) of omnidirectional PDPs and PAS (polar plots) were generated, and the primary and secondary statistics were extracted using the same 2.7 ns inter-cluster void duration and 20 dB PAS thresholding procedure to compare with the measured statistics. Fig. 8 shows the measured vs. simulated omnidirectional RMS delay spreads from measured 28 GHz NLOS data. We also show the CDF of the NLOS RMS delay spreads obtained from measured PDPs using directional antennas over 10° angle increments for comparison. Table I, Table II, and Table III present and compare the generated statistics from the simulator with the actual measured statistics. The simulated omnidirectional path loss model provides good agreement with the measured omnidirectional path loss model. The means of simulated temporal and spatial primary statistics are all within 10% of the measured means, and the simulated distributions remained identical to the measured distributions. The reproduced simulated statistics indicate that the statistical simulator presented can accurately reproduce the statistics of the 28 GHz dense urban NLOS measured channels.

III. CONCLUSION

A statistical omnidirectional channel model offering joint temporal and spatial statistics for 28 GHz ultra-wideband propagation in dense urban NLOS environments was presented based upon real-world measurements in Manhattan. A statistical simulator was shown to recreate accurate and faithful channel statistics and PDPs. This statistical simulator can be used for system-wide simulations, just as the 3GPP and WINNER II models have been used at lower frequencies. Additional models incorporating angle of departure statistics, as well as NLOS weak diffuse scattering will improve and

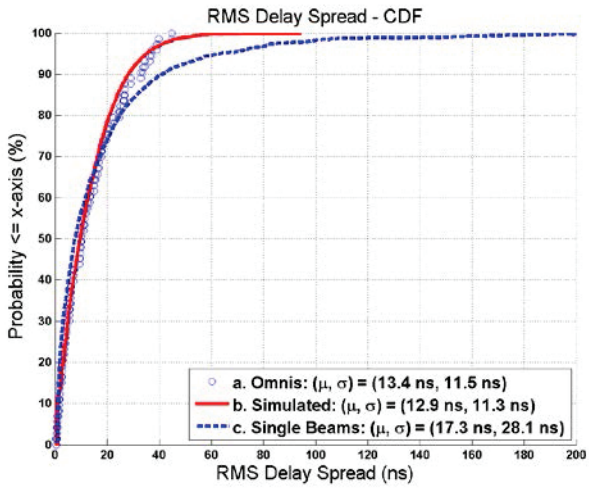

Fig. 8: Cumulative distribution of RMS delay spread for a) simulated omnidirectional PDPs using the procedure in Section II.A; b) the measured omnidirectional PDPs based on synthesized propagation time, and c) the entire NLOS measurement database using rotating horn antennas in [2][3]. The three curves are in close agreement, with higher delay spreads occurring with directional antennas.

enhance the presented SSCM. Similar models are needed for mmWave frequency bands to extend the presented channel modeling framework at higher frequencies.

ACKNOWLEDGMENT

This work was sponsored by Samsung DMC R&D Communications Research Team (CRT) through Samsung Telecommunications America, LLC, and the NYU WIRELESS Industrial Affiliates.

TABLE I: SUMMARY OF MEASURED AND SIMULATED OMNIDIRECTIONAL PATH LOSS MODEL WITH RESPECT TO A 1 M FREE SPACE REFERENCE USING 10,000 SIMULATED PDPS AND PAS. (P) AND (S) STAND FOR PRIMARY AND SECONDARY, RESPECTIVELY.

Path Loss Model	Measured (n, σ)	Simulated (n, σ)	Error (%)
Omnidirectional (P)	(3.4, 9.7 dB)	(3.4, 9.8 dB)	(0, 1.0)

TABLE II:SUMMARY OF THE MEASURED STATISTICS WERE OBTAINED FROM 28 GHZ OMNIDIRECTIONAL WIDEBAND PDPS, AND THE SIMULATED STATISTICS WERE GENERATED FROM 10,000 PDPS AND PAS OBTAINED FROM A STATISTICAL SIMULATOR IMPLEMENTING THE STEP PROCEDURE PRESENTED IN II.A. (P) AND (S) STAND FOR PRIMARY AND SECONDARY, RESPECTIVELY.

Type of Statistic	Quantity	Measured (μ, σ)	Simulated (μ, σ)	Error (%)
Temporal	Number of Clusters (P)	Poisson (3.4, 2.1)	(3.2, 2.1)	(5.9, 0)
	Number of Cluster Subpaths (P)	Exponential (2.1, 1.6)	(2.2, 1.7)	(4.7, 6.3)
	Cluster Excess Time Delay (ns) (P)	Exponential (66.3, 68.0)	(71.8, 62.1)	(8.3, 8.7)
	Cluster Subpath Excess Time Delay (ns) (P)	Exponential (8.1, 8.8)	(8.6, 8.0)	(6.2, 9.1)
	RMS Delay Spread (ns) (S)	Exponential (13.4, 11.5)	(12.9, 11.3)	(3.7, 1.7)
	Cluster RMS Delay Spread (ns) (S)	Exponential (2.0, 2.0)	(2.4, 1.7)	(20.0, 15.0)
	Cluster Duration (ns) (S)	Exponential (8.9, 8.7)	(10.7, 8.4)	(20.2, 3.5)
	Inter-cluster Void Duration (ns) (S)	Exponential (16.8, 17.2)	(21.5, 15.9)	(28.0, 7.5)
Spatial	Number of Lobes (P)	Poisson (2.4, 1.3)	(2.3, 1.1)	(4.2, 15.4)
	AOA (°) (P)	*Unif*(0, 360)	*Unif*(0, 360)	0
	Lobe Azimuth Spread (°) (P)	Normal (34.8, 25.7)	(34.6, 27.8)	(0.2, 9.0)
	RMS Lobe Azimuth Spread (°) (S)	Exponential (6.1, 5 .8)	(8.3, 6.8)	(36, 17)

TABLE III: SUMMARY OF MEASURED AND SIMULATED CLUSTER AND CLUSTER SUBPATH POWER RATIOS GENERATED FROM 10,000 PDPS. α AND β ARE DEFINED IN STEP 7 AND 8 OF II.A (P) STANDS FOR PRIMARY.

Type of Statistic	Quantity	Measured $(\alpha, \beta[ns])$	Simulated $(\alpha, \beta[ns])$	Error (%)
Temporal	Cluster Power Ratio (P)	$(0.613, 31.4)$	$(0.584, 41.3)$	(4.7, 35.7)
	Cluster Subpath Power Ratio (P)	$(0.966, 6.63)$	$(0.859, 5.02)$	(11.1, 24.3)

REFERENCES

[1] N.S. Networks, "2020: Beyond 4G: Radio Evolution for the Gigabit Experience," 2011.

[2] T. S. Rappaport, S. Sun, R. Mayzus, H. Zhao, Y. Azar, K. Wang, G. N. Wong, J. K. Schulz, M. K. Samimi and F. Gutierrez, "Millimeter Wave Mobile Communications for 5G Cellular: It Will Work!," *IEEE Access,* vol. 1, pp. 335-349, 2013.

[3] Y. Azar, G. N. Wong, R. Mayzus, J. K. Schulz, H. Zhao, F. J. Gutierrez, D. Hwang and T. S. Rappaport, "28 GHz Propagation Measurements for Outdoor Cellular Communications Using Steerable Beam Antennas in New York City," *IEEE International Conference on Communications (ICC),* 9-13 June 2013.

[4] A. F. Molisch, H. Asplund, R. HedderGott, M. Steinbauer and T. Zwick, "The COST259 Directional Channel Model - Part I: Overview and Methodology," *IEEE Transactions on Wireless Communications,* vol. 5, no. 12, pp. 3421-3433, December 2006.

[5] IST-WINNER D1.1.2P. Kyosti, et al., "WINNER II Channel Models," ver1.1 September 2007.

[6] V6.1.0, 3GPP TR 25.996, "Spatial Channel Model for Multipath Input Multiple Output (MIMO) Simulations," September 2003.

[7] M. K. Samimi, K. Wang, Y. Azar, G. N. Wong, R. Mayzus, H. Zhao, S. Sun, F. Gutierrez and T. S. Rappaport, "28 GHz Angle of Arrival and Angle of Departure Analysis for Outdoor Cellular Communications using Steerable Beam Antennas in New York City," *IEEE Vehicular Technology Conference (VTC),* 2-5 June 2013.

[8] M. K. Samimi and T. S. Rappaport, "Characterization of the 28 GHz Millimeter-Wave Dense Urban Channel for Future 5G Mobile Cellular," *Technical Report, TR 2014-001,* June 2014.

[9] T. S. Rappaport, F. Gutierrez, E. Ben-Dor, J. Murdock, Y. Qiao and J. Tamir, "Broadband Millimeter-Wave Propagation Measurements and Models Using Adaptive-Beam Antennas for Outdoor Urban Cellular Communications," *IEEE Transactions on Antennas and Propagation,* vol. 61, no. 4, pp. 1850-1859, April 2013.

[10] S. Rangan, T. S. Rappaport and E. Erkip, "Millimeter-wave cellular wireless networks: potentials and challenges," *Proceedings of the IEEE,* vol. 102, no. 3, pp. 366-385, March 2014.

[11] M. G. Bulmer, Principles of Statistics, p. 154, The M.I.T. Press, 1965.

[12] W. H. Tranter, K. S. Shanmugan, T. S. Rappaport and K. L. Kosbar, Principles of Communication Systems Simulation with Wireless Applications, Prentice Hall Communications Engineering and Emerging Technologies Series, 2004..